

# Fractional quantum anomalous Hall effect in a singular flat band

Wenqi Yang,<sup>1</sup> Dawei Zhai,<sup>1</sup> Tixuan Tan,<sup>2</sup> Feng-Ren Fan,<sup>1</sup> Zuzhang Lin,<sup>1</sup> and Wang Yao<sup>1,\*</sup>

<sup>1</sup>*New Cornerstone Science Laboratory, Department of Physics,  
The University of Hong Kong, Hong Kong, China*

<sup>2</sup>*Department of Physics, Stanford University, Stanford, CA 94305, USA*

In the search of fractional quantum anomalous Hall (FQAH) effect, the conventional wisdom is to start from a flat Chern band isolated from the rest of the Hilbert space by band gaps, so that many-body interaction can be projected to a landscape that mimics a Landau level. Singular flat bands (SFB), which share protected touching points with other dispersive bands, represent another type of flat landscapes differing from Landau levels and Chern bands in topological and geometric properties. Here we report the finding of FQAH phases in a SFB, which emerges in the bipartite limit of the nearest-neighbor tight-binding model of twisted bilayer MoTe<sub>2</sub>. At 1/3 and 2/3 filling of the SFB, FQAH effects are demonstrated using density matrix renormalisation group calculations with all bands, as well as exact diagonalization calculations with the two touching bands. Gapping the band touching can turn the SFB into a nearly flat Chern band, but counter-intuitively this suppresses the FQAH effect, as the gap opening introduces strong inhomogeneity to the quantum geometry. An optical scheme to realize such SFB for cold atoms is provided. Our findings uncover a new arena for the exploration of fractional quantum Hall physics beyond the Landau level and Chern insulator paradigms.

Quantum anomalous Hall effects, the zero-magnetic-field analog of the quantum Hall effects, are widely explored in magnetic topological insulators [1–3]. These insulators host Bloch bands of nonzero Chern numbers that resemble Landau levels in an applied magnetic field [4], leading to the observations of integer quantum anomalous Hall effects [5–8]. Besides topology, another important aspect of Landau levels is their flatness in dispersion and quantum geometry, as well as isolation by energy gaps. This underlies the emergence of fractional quantum Hall effects when many-body interaction projected to individual Landau levels dominates the electron correlation at fractional fillings [9]. The search for fractional quantum anomalous Hall (FQAH) effect has therefore naturally started from insulators having a flat Chern band well isolated from all other bands by energy gaps. There has been a remarkable surge of research to engineer such band Chern insulators in various lattice models [10–18], where FQAH phases (or fractional Chern insulators [16]) are revealed under short-range interactions by exact diagonalization (ED) or density matrix renormalization group (DMRG) calculations. Most notably, experimental observations of FQAH effects are recently reported in the isolated Chern band of twisted rhombohedral bilayers of MoTe<sub>2</sub> [19–22] and pentalayer graphene/hBN moiré [23], which are significantly advancing the research field.

The emergence of flat topological band is subject to fundamental constraints. In 2D lattices of finite-ranged hopping, a Bloch band can not simultaneously possess exact flatness, nonzero Chern number, and isolation by energy gap [24]. In a variety of lattice models, such constraint underlies another intriguing context for the exploration of strong correlation and topological physics, i.e. *singular flat band* (SFB), where exact band flatness is protected by point touching with dispersive band(s)

[25–27]. These lattices host two types of states localized by destructive hopping interference [25]: compact localized states of 0D character; and 1D states forming non-contractible loops encircling the torus geometry under periodic boundary condition. Contribution of the non-contractible loop states to the state counting at the flat-band energy dictates the presence of the point touching as immovable singularity of the band [25–27]. In applied magnetic fields, a SFB can develop Landau levels at unexpected energies, and exhibit diverging orbital magnetic susceptibility [28]. Along with these exotic single-particle properties, the exact band flatness offers prospects for strong correlation physics. However, the band touching is often considered to be troublesome, rendering the projection onto the flat band problematic and band Chern number undefinable.

In this work we report the finding of FQAH states in a SFB, which emerges in the bipartite limit of the nearest-neighbor tight-binding model of twisted bilayer MoTe<sub>2</sub> [29]. At 1/3 and 2/3 fillings of the SFB, FQAH effects are demonstrated with real-space DMRG calculations taking into account all bands with nearest-neighbor repulsive interaction ( $U_1$ ). ED calculations on the two touching bands corroborate the DMRG results and reveal that the FQAH states are predominantly weighted in the SFB. For FQAH phases at both fillings, lower bound in  $U_1$  is not observed within our computation capacity, consistent with the exact band flatness. Analysis of the ground state wave functions, as well as Hartree-Fock bands at the closest integer fillings, suggests that interaction-driven gap opening of the band touching is the cause for the transition from FQAH to a topologically trivial phase with the increase of  $U_1$ , which occurs at very different  $U_1$  magnitudes at 1/3 and 2/3 SFB fillings. Gapping the band touching turns the SFB into a

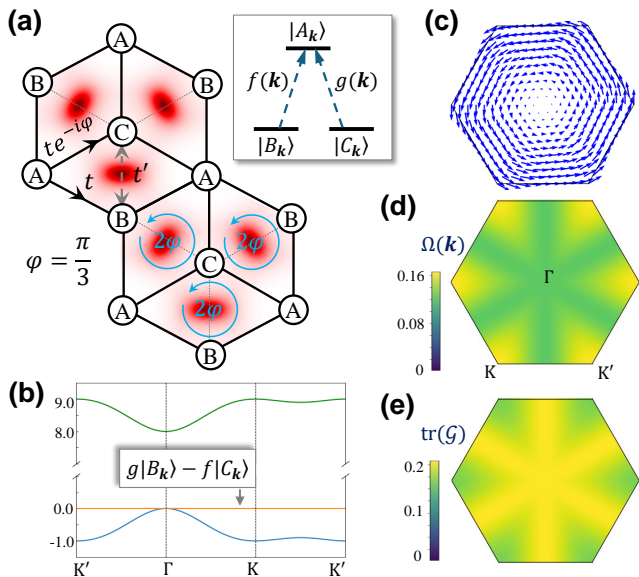


FIG. 1. (a) Schematics of the dice lattice, with red color in the background denoting a pseudo-magnetic field (see Fig. 4). Inset: at an arbitrary wave vector  $\mathbf{k}$ , coupling between the three orbitals realizes a  $\Lambda$  scheme. (b) Band structure in the non-interacting limit. (c) Under a non-periodic atomic gauge (see text), Berry connection of the SFB is continuous at the touching point  $\Gamma$ . (d) Berry curvature  $\Omega$  and (e) trace of quantum metric tensor  $\mathcal{G}$  of the SFB. Here  $E_A = 8$ , and the lattice constant is set to 1. All energies here and hereafter are measured in units of the hopping amplitude  $t$ .

nearly flat isolated Chern band, but counter-intuitively this destroys the FQAH state as the gap opening introduces strong inhomogeneity to the quantum geometry. We also present a scheme to realize such SFB in optical lattice.

**SFB model and its quantum geometry** – A minimal model for realizing SFBs with nearest-neighbor hopping is a three-orbital one with the Bloch Hamiltonian (see Supplemental Material [30])

$$\hat{H}_0(\mathbf{k}) = E_A \hat{A}_\mathbf{k}^\dagger \hat{A}_\mathbf{k} + f(\mathbf{k}) \hat{A}_\mathbf{k}^\dagger \hat{B}_\mathbf{k} + g(\mathbf{k}) \hat{A}_\mathbf{k}^\dagger \hat{C}_\mathbf{k} + h.c.. \quad (1)$$

This generic model has a flat band at the zero energy, where the unnormalized Bloch state  $|\psi_{\text{flat}}\rangle = (0, g, -f)^T$  has no weight on A orbitals.  $f(\mathbf{k})$  and  $g(\mathbf{k})$  are determined by the lattice geometry and hopping phases, and when they simultaneously vanish at a  $\mathbf{k}$  point, a band touching with other dispersive band(s) occurs as an immovable singularity [26, 27]. Such touching is protected by the topology in real space that leads to over-completeness of zero modes [25, 26]. We consider an example of such nearest-neighbor hopping SFB model on a

dice lattice geometry [31, 32],

$$\begin{aligned} \hat{H}_0 = & \sum_l E_A \hat{A}_l^\dagger \hat{A}_l \\ & - \sum_{\langle l,m \rangle} \left( t e^{i\phi_1^{l,m}} \hat{A}_l^\dagger \hat{B}_m + t e^{i\phi_2^{l,m}} \hat{A}_l^\dagger \hat{C}_m + h.c. \right), \end{aligned} \quad (2)$$

with a  $2\pi/3$  flux threading each rhombus [Fig. 1(a)]. This corresponds to the bipartite limit of the nearest-neighbor tight-binding model of twisted bilayer  $\text{MoTe}_2$  [29], where A orbital detuning  $E_A > 0$ , and the flux is from real-space Berry curvature in the moiré. The hopping between B and C orbitals has a small amplitude in twisted  $\text{MoTe}_2$  [33], and is switched off here. One identifies

$$\begin{aligned} f(\mathbf{k}) &= -t \left( e^{-i\mathbf{k}\cdot\mathbf{d}_1} + e^{i2\pi/3} e^{-i\mathbf{k}\cdot\mathbf{d}_2} + e^{-i2\pi/3} e^{-i\mathbf{k}\cdot\mathbf{d}_3} \right) \\ g(\mathbf{k}) &= t \left( e^{i\mathbf{k}\cdot\mathbf{d}_1} + e^{i2\pi/3} e^{i\mathbf{k}\cdot\mathbf{d}_2} + e^{-i2\pi/3} e^{i\mathbf{k}\cdot\mathbf{d}_3} \right) \end{aligned} \quad (3)$$

where  $\mathbf{d}_{1,2,3}$  are nearest-neighbor vectors from A to B orbitals.  $f$  and  $g$  both vanish at the  $\Gamma$  point, leading to a quadratic band touching with the lower dispersive band when  $E_A > 0$  [Fig. 1(b)]. The overcomplete set of zero modes, including compact localized states and non-contractible loop states, is illustrated in supplementary Fig. S1 [30], which are the defining characters of a SFB [25, 26].

Interestingly, the SFB here exhibits features of a Chern band. While ill-defined at the  $\Gamma$  point, the Berry curvature  $\Omega$  and quantum metric tensor  $\mathcal{G}$  are smooth and nearly uniform everywhere else [Figs. 1(d, e)]. The integral of  $\Omega$  without the  $\Gamma$  point yields  $2\pi$  on the SFB, and  $-2\pi$  on the lower dispersive band. Upon a singular non-periodic gauge transformation  $|\psi'_{\text{flat}}\rangle = e^{-i\theta} |\psi_{\text{flat}}\rangle$ , where  $\theta$  is the polar angle of  $\mathbf{k}$ , the normalized Bloch state  $|\psi'_{\text{flat}}\rangle$  is continuous, which approaches  $(0, -i, i)^T/\sqrt{2}$  from all directions towards  $\Gamma$ . In this gauge, the berry connection  $\mathbf{A}' = i \langle \psi'_{\text{flat}} | \nabla \psi'_{\text{flat}} \rangle$  also becomes continuous and smooth around  $\Gamma$  [Fig. 1(c)] (see Supplementary Material [30]). We also note that the maximum quantum distance [28] between Bloch states around the  $\Gamma$  point is vanishing here, which also distinguishes this SFB from existing cases [27].

**FQAH effect at fractional SFB fillings** – To properly account for the effect of band touching in the many-body correlation, we perform real-space DMRG calculations with the tight-binding Hamiltonian Eq. (2) and nearest-neighbor repulsion  $H_{\text{int}} = \sum_{\langle l,m \rangle} U_1^{l,m} \hat{n}_l \hat{n}_m$  of spinless fermions, on a cylinder geometry (details in Supplemental Materials [30]). We find FQAH phases at  $1/3$  and  $2/3$  fillings of the SFB, which are signified by fractionally quantized charge pumping between open boundaries of the cylinder upon the adiabatic flux insertion.

Figure 2(a) presents an example of the charge pumping at SFB filling factor  $\nu_{\text{sfb}} = 2/3$  (the total filling factor  $\nu = \nu_{\text{sfb}} + 1 = 5/3$ ). One charge quantum is pumped after

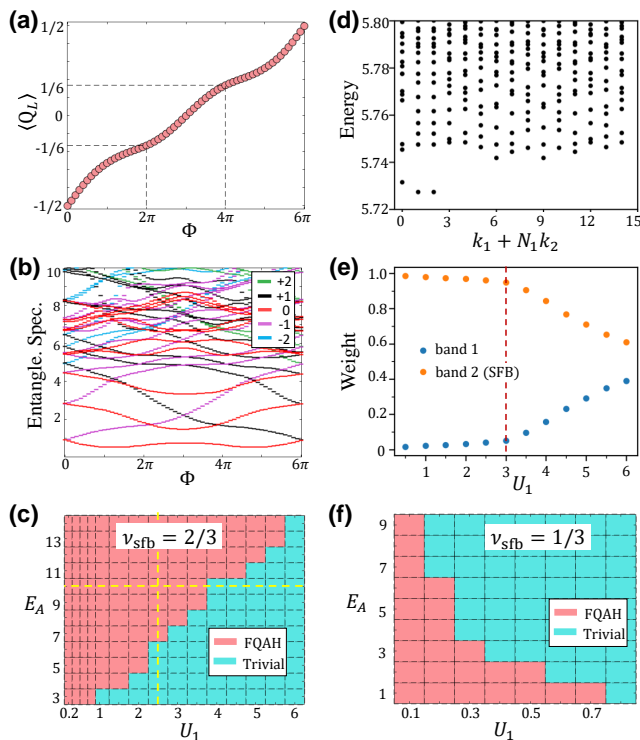


FIG. 2. (a–c) Real-space DMRG calculations accounting all bands at  $\nu_{\text{sfb}} = 2/3$ : FQAH effect demonstrated by charge pumping (a) and entanglement spectrum flow (b) upon flux insertion, at  $E_A = 10$ ,  $U_1 = 1.5$ ; (c)  $E_A$ - $U_1$  phase diagram, magenta color denotes the FQAH phase, and blue for a topologically trivial phase. (d–e) ED calculations on the two touching bands at  $\nu_{\text{sfb}} = 2/3$ : (d) many-body eigenspectrum at  $E_A = 10$ ,  $U_1 = 0.5$ ; (e) band projections of the ground states at  $E_A = 10$  (corresponding eigenspectra in supplementary Fig. S7). (f) Phase diagram at  $\nu_{\text{sfb}} = 1/3$  from DMRG.

three flux periods, signaling a fractionally quantized Hall conductivity of  $e^2/(3h)$  [34]. The entanglement spectrum flow in Fig. 2(b) also provides evidence for a  $1/3$  quantized charge pumping per cycle: the spectrum is shifted by one particle sector after  $6\pi$  flux insertion. Figure 2(c) presents the phase diagram at  $\nu_{\text{sfb}} = 2/3$  in the parameter space spanned by the interaction strength  $U_1$  and onsite energy  $E_A$ . It consists of the FQAH phase in a wide parameter space characterized by the  $1/3$  quantized charge pumping, and a trivial metallic phase of vanishing charge gap. The phase boundary is also corroborated by the discontinuity in entanglement spectrum [35, 36], as shown in supplementary Fig. S2 [30] for the scans along the vertical and horizontal dashed lines in Fig. 2(c).

We also perform two-band ED calculations which provide complementary information that corroborates the DMRG findings. Figure 2(e) presents the band projection of the ground states at  $E_A = 10$  with various  $U_1$ , and the corresponding many-body eigenspectra are shown in Fig. 2(d) and supplementary Fig. S7. For  $U_1 < 3$ , the spectra show characteristics of FQAH phase, agree-

ing well with the DMRG phase diagram in Fig. 2(c). Interestingly, these FQAH ground states are predominantly weighted in the SFB, despite the band touching and strong interaction exceeding the spectral window spanned by the two touching bands. This is reminiscent of the findings in certain Chern insulator models where FQAH states exist and weight predominantly on the flat Chern band when interaction strength well exceeds the band gap [37, 38]. Upon transition to the metallic phase, the weight on the dispersive band starts to grow rapidly.

At  $\nu_{\text{sfb}} = 1/3$  (total filling  $\nu = 4/3$ ), FQAH phase is also found, but in a narrow region where  $U_1$  is small [Fig. 2(f)]. In this FQAH phase, two charge quanta are pumped upon  $6\pi$  flux insertion (supplementary Fig. S4), corresponding to a fractionally quantized Hall conductivity of  $2e^2/(3h)$ . At both  $\nu_{\text{sfb}} = 1/3$  and  $2/3$ , the lower boundary of FQAH phase as function of interaction strength  $U_1$  is not observed within our computation capacity. The phase diagrams start from  $U_1 = 0.1 \sim 0.2$ , below which the small charge gap demands larger bond dimension for convergence.

**Band touching and stability of FQAH** – For both  $\nu_{\text{sfb}} = 1/3$  and  $2/3$  FQAH phases, transition to a topologically trivial phase occurs upon the increase of interaction strength, but the  $\nu_{\text{sfb}} = 2/3$  FQAH phase is obviously more robust with a much larger upper critical  $U_1$ . To elucidate this sharp contrast, self-consistent Hartree-Fock calculations are performed at the closest integer fillings (supplementary Fig. S5), where the interaction-renormalized quasiparticle bands can in general provide some insight.  $\nu_{\text{sfb}} = 1/3$  corresponds to  $1/3$  particle added to the empty SFB at  $\nu = 1$ . At this integer filling, as  $U_1$  is ramped up, the Hartree-Fock mean field leads to a small gap  $\Delta_\Gamma$  at the band touching [supplementary Fig. S5(a)], whose contour line shows remarkable resemblance to the FQAH phase boundary at  $\nu_{\text{sfb}} = 1/3$ . We note the Fock term manifests as an effective hopping  $t'_{\text{eff}}(\hat{B}_l^\dagger \hat{C}_m + h.c.)$ , with  $t'_{\text{eff}}$  proportional to  $U_1$  and the nearest-neighbour inter-orbital coherence  $\langle C_m^\dagger B_l \rangle$ . The Hartree term generates an energy offset  $\delta_{\text{eff}}$ , between the B and C orbitals, proportional to the inter-orbital polarization. Either term can gap the touching point [cf. Fig. 3(c, d)].

$\nu_{\text{sfb}} = 2/3$  can be considered as  $1/3$  hole added on top of the full SFB filling at  $\nu = 2$ . With B and C orbitals near fully filled, especially at large A orbital detuning, the inter-orbital coherence and polarization at  $\nu = 2$  have tiny magnitudes compared to the  $\nu = 1$  case, therefore opening a comparable  $\Delta_\Gamma$  requires a much larger  $U_1$ . This is in line with the stability of  $\nu_{\text{sfb}} = 2/3$  FQAH phase against the increase of  $U_1$ .

Analysis of the ground state wave functions at the fractional fillings from DMRG calculations supports the observation that gapping of touching point in the interaction renormalized band accompanies the quench of the FQAH effect. In supplementary Fig. S3, the evolution of

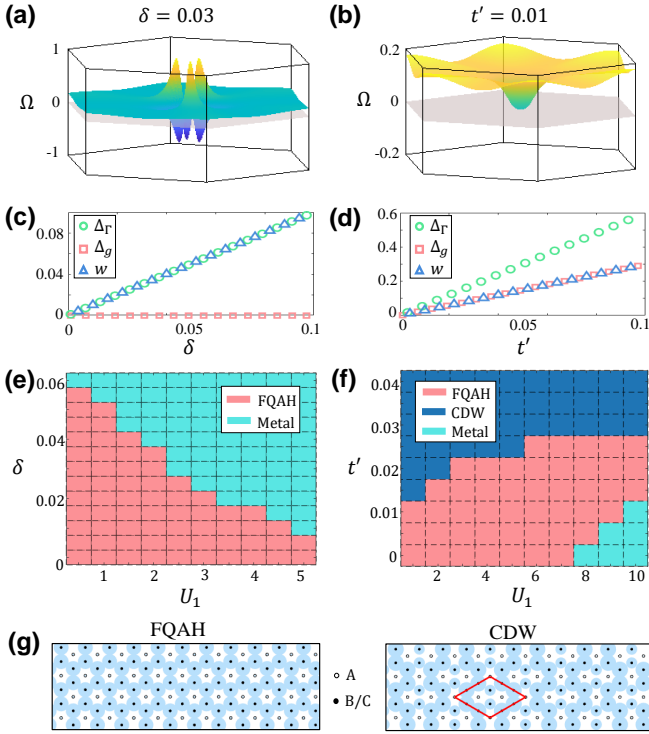


FIG. 3. **Breaking of band touching and stability of FQAH effect.** (a, b) Berry curvature distribution in the perturbed flat band, when the band touching is gapped by an energy offset  $\delta$  or small hopping  $t'$  between B and C orbitals. (c, d) Bandgap ( $\Delta_g$ ) between the two lower bands, their gap at  $\Gamma$  point ( $\Delta_\Gamma$ ), and bandwidth of the perturbed flat band ( $w$ ), as functions of  $\delta$  and  $t'$ . (e)  $U_1$ - $\delta$  phase diagram at  $\nu_{\text{sfb}} = 2/3$ ,  $t' = 0$ ,  $E_A = 15$ . (f)  $U_1$ - $t'$  phase diagram at  $\nu_{\text{sfb}} = 2/3$ ,  $\delta = 0$ ,  $E_A = 15$ . FQAH, metallic and CDW phases are denoted by magenta, light blue and dark blue colors respectively. (g) Examples of charge distributions of FQAH phase and CDW phase. Particle populations on each orbitals are denoted by the size of the blue circles. Red diamond denotes the  $\sqrt{3} \times \sqrt{3}$  supercell in the CDW state.

the many-body charge gap at  $\nu_{\text{sfb}} = 2/3$  as a function of  $U_1$  is plotted along with the polarization between B and C orbitals. After a critical  $U_1$  within the FQAH phase, weak orbital polarization and thus a finite  $\delta_{\text{eff}}$  through the Hartree term spontaneously emerges [supplementary Fig. S3(d)], coinciding with the decrease of the many-body charge gap. The transition from FQAH to the trivial metallic phase is accompanied by a further significant increase in the orbital polarization [supplementary Fig. S3(d)].

We note that gapping the band touching by either the  $t'_{\text{eff}}$  or  $\delta_{\text{eff}}$  term turns the SFB into an isolated Chern band with nearly flat dispersion [supplementary Fig. S5(f)]. However, this comes at the cost of a strong inhomogeneity in the Berry curvature [cf. Figs. 3(a, b)]. With a larger gap, the inhomogeneity is spread out over a larger  $k$ -space region, which is unfavorable for FQAH state to form [39, 40].

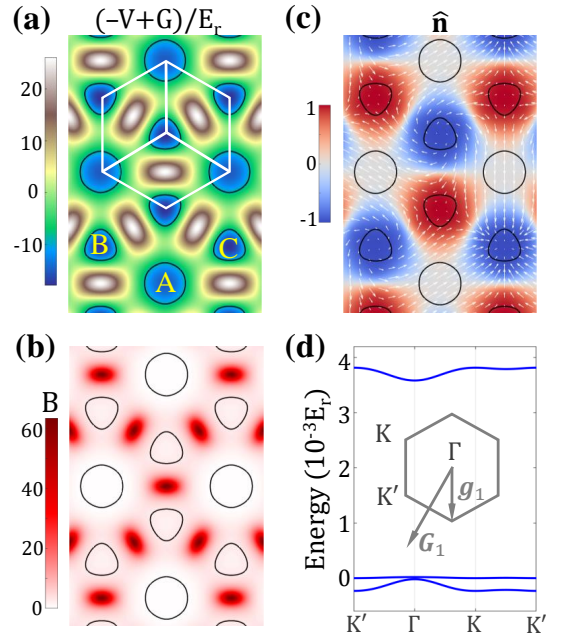


FIG. 4.  **$2\pi$ -flux dice lattice and SFB for ultracold atoms.** (a) Potential landscape in units of  $E_r = \frac{\hbar^2}{2m}|G_1|^2$ . The energy has been shifted to place the barrier height between A and B/C sites at 0. (b) Pseudo-magnetic field rescaled by unit cell area and flux quantum. The flux per unit cell is  $2\pi$ . (c) Spatial texture of  $\hat{\mathbf{n}}$ . Background color denotes  $n_z$ , and arrows for in-plane vector  $(n_x, n_y)$ . (d) Energy bands under  $V_0 \approx -19.75E_r$  and  $V_1 \approx -23.8E_r$ . The energies have been shifted to place the flat band around zero energy.

The counter-intuitive role of band touching is further corroborated by examining phase diagram upon adding the B-C hopping  $t'(\hat{B}_i^\dagger \hat{C}_m + h.c.)$  and energy offset  $\delta$  to the single-particle Hamiltonian  $\hat{H}_0$ . Figure 3(e) shows the phase diagram in  $U_1$ - $\delta$  space, fixing  $E_A = 15$ . A small  $\delta$  to gap the touching point in the single-particle bands can significantly reduce the stability of FQAH phase against the increase of interaction strength. Figure 3(f) shows the phase diagram in  $U_1$ - $t'$  space at  $E_A = 15$ . When  $t'$  is small, a transition from FQAH to metallic phase at large  $U_1$  is also observed, as a continuation of the  $t' = 0$  phase diagram. In this regime  $t'$  can push the FQAH to metal transition towards a larger  $U_1$ . Increasing  $t'$  slightly further destroys the FQAH phase and drives the system into a  $\sqrt{3} \times \sqrt{3}$  charge density wave (CDW). Figure 3(g) shows examples of the carrier distributions in FQAH and CDW phases respectively.

All these comparisons and analysis suggest that the FQAH states here are inherently associated with the SFB rather than an interaction renormalized isolated Chern band. The FQAH effect exists here in the weak  $U_1$  limit where the Hartree-Fock bands fully retain the SFB feature, and in the moderate  $U_1$  regime where the band touching is minimally gapped. This finding is in stark contrast to existing paradigms, where opening of a sizable

gap by interaction [41–44] or single-particle effect [45] to isolate a Chern band is favorable for the FQAH states.

#### Realization of the SFB in optical lattice –

We generalize here the optical flux lattice scheme initially proposed in Ref. [46]. Consider atoms of two long-lived levels moving in optical fields:  $\hat{H} = \frac{\hat{p}^2}{2m} - \mathbf{V}(\mathbf{r}) \cdot \hat{\boldsymbol{\sigma}}$ , where  $\hat{\boldsymbol{\sigma}}$  is the vector of Pauli matrices. The off-diagonal  $V_{x,y}$  are the interspecies optical coupling generated with three travelling waves [46]:  $V_x = V_0 \sum_{i=1}^3 \cos(\mathbf{g}_i \cdot \mathbf{r})$ ,  $V_y = -V_0 \sum_{i=1}^3 \sin(\mathbf{g}_i \cdot \mathbf{r})$ .  $V_z$  corresponds to a species-dependent optical potential, which we consider a form generated by three standing waves:  $V_z = -V_1 \sum_{i=1}^3 \sin(\mathbf{G}_i \cdot \mathbf{r})$ . The wavevectors  $\mathbf{G}_1 = -(\frac{1}{\sqrt{3}}, 1) \frac{2\pi}{L}$  and  $\mathbf{g}_1 = -(0, \frac{2}{3}) \frac{2\pi}{L}$  [Fig. 4(d)], and  $\mathbf{G}_{2,3}$  and  $\mathbf{g}_{2,3}$  are their 120° degree rotations respectively. The magnitude and direction of  $\mathbf{V}$  will be denoted by  $V(\mathbf{r})$  and  $\hat{\mathbf{n}}(\mathbf{r})$ .

Adiabatic motion on the local ground states with Bloch vectors along  $\hat{\mathbf{n}}(\mathbf{r})$  is then governed by an effective Hamiltonian:  $\hat{H}_{\text{adb}} = \frac{1}{2m} [\hat{\mathbf{p}} + e\mathbf{A}(\mathbf{r})]^2 - V(\mathbf{r}) + G(\mathbf{r})$  where atoms experience a periodic scalar potential with geometric correction  $G = \frac{\hbar^2}{8m} (\nabla \hat{\mathbf{n}})^2$  [47], and a pseudo-magnetic field  $\mathbf{B} = \nabla \times \mathbf{A} = \frac{\hbar}{2e} \hat{\mathbf{n}} \cdot (\partial_x \hat{\mathbf{n}} \times \partial_y \hat{\mathbf{n}}) \mathbf{z}$ . The magnetic flux threading a unit cell equals  $2\pi$ , as determined by the solid angle enclosed by  $\hat{\mathbf{n}}$ . For the example in Fig. 4, the three local minima in the potential landscape define the orbitals, where tunneling between the degenerate B and C sites is suppressed by a significant barrier [Fig. 4(a)], realizing a  $2\pi$ -flux dice lattice. The lowest three energy bands [Fig. 4(d)] indeed reproduce all features of the non-interacting tight-binding Hamiltonian featuring the SFB. This cold atom platform offers a clean and tunable arena to examine the counter-intuitive role of band touching in stabilizing FQAH in the SFB.

**Acknowledgment** – We thank Bin-Bin Chen, Wei Zheng, Zhen Zheng, Jie Wang and Qian Niu for helpful discussions. Wenqi Yang thanks Tao Xiang, Kang Wang and Runze Chi for guidance on learning DMRG. The work is supported by Research Grant Council of Hong Kong SAR (HKU SRFS2122-7S05, AoE/P-701/20, A-HKU705/21), and New Cornerstone Science Foundation.

---

\* wangyao@hku.hk

- [1] F. D. M. Haldane, Model for a quantum hall effect without landau levels: Condensed-matter realization of the "parity anomaly", *Phys. Rev. Lett.* **61**, 2015 (1988).
- [2] Y. Tokura, K. Yasuda, and A. Tsukazaki, Magnetic topological insulators, *Nat. Rev. Phys.* **1**, 126 (2019).
- [3] C.-Z. Chang, C.-X. Liu, and A. H. MacDonald, Colloquium: Quantum anomalous hall effect, *Rev. Mod. Phys.* **95**, 011002 (2023).
- [4] D. J. Thouless, M. Kohmoto, M. P. Nightingale, and M. den Nijs, Quantized hall conductance in a two-dimensional periodic potential, *Phys. Rev. Lett.* **49**, 405 (1982).
- [5] C.-Z. Chang, J. Zhang, X. Feng, J. Shen, Z. Zhang, M. Guo, K. Li, Y. Ou, P. Wei, L.-L. Wang, *et al.*, Experimental observation of the quantum anomalous hall effect in a magnetic topological insulator, *Science* **340**, 167 (2013).
- [6] Y. Deng, Y. Yu, M. Z. Shi, Z. Guo, Z. Xu, J. Wang, X. H. Chen, and Y. Zhang, Quantum anomalous hall effect in intrinsic magnetic topological insulator MnBi<sub>2</sub>Te<sub>4</sub>, *Science* **367**, 895 (2020).
- [7] M. Serlin, C. L. Tschirhart, H. Polshyn, Y. Zhang, J. Zhu, K. Watanabe, T. Taniguchi, L. Balents, and A. F. Young, Intrinsic quantized anomalous hall effect in a moiré heterostructure, *Science* **367**, 900 (2020).
- [8] T. Li, S. Jiang, B. Shen, Y. Zhang, L. Li, Z. Tao, T. Devakul, K. Watanabe, T. Taniguchi, L. Fu, J. Shan, and K. F. Mak, Quantum anomalous hall effect from intertwined moiré bands, *Nature* **600**, 641 (2021).
- [9] B. I. Halperin and J. K. Jain, *Fractional quantum Hall effects: new developments* (World Scientific, Singapore, 2020).
- [10] E. Tang, J.-W. Mei, and X.-G. Wen, High-temperature fractional quantum hall states, *Phys. Rev. Lett.* **106**, 236802 (2011).
- [11] Y.-L. Wu, B. A. Bernevig, and N. Regnault, Zoology of fractional chern insulators, *Phys. Rev. B* **85**, 075116 (2012).
- [12] K. Sun, Z. Gu, H. Katsura, and S. D. Sarma, Nearly flatbands with nontrivial topology, *Phys. Rev. Lett.* **106**, 236803 (2011).
- [13] T. Neupert, L. Santos, C. Chamon, and C. Mudry, Fractional quantum hall states at zero magnetic field, *Phys. Rev. Lett.* **106**, 236804 (2011).
- [14] D. Sheng, Z.-C. Gu, K. Sun, and L. Sheng, Fractional quantum hall effect in the absence of landau levels, *Nat. Commun.* **2**, 389 (2011).
- [15] Y.-F. Wang, Z.-C. Gu, C.-D. Gong, and D. Sheng, Fractional quantum hall effect of hard-core bosons in topological flat bands, *Phys. Rev. Lett.* **107**, 146803 (2011).
- [16] N. Regnault and B. A. Bernevig, Fractional chern insulator, *Phys. Rev. X* **1**, 021014 (2011).
- [17] D. Xiao, W. Zhu, Y. Ran, N. Nagaosa, and S. Okamoto, Interface engineering of quantum hall effects in digital transition metal oxide heterostructures, *Nat. Commun.* **2**, 596 (2011).
- [18] J. W. Venderbos, S. Kourtis, J. van den Brink, and M. Daghofer, Fractional quantum-hall liquid spontaneously generated by strongly correlated t2g electrons, *Phys. Rev. Lett.* **108**, 126405 (2012).
- [19] J. Cai, E. Anderson, C. Wang, X. Zhang, X. Liu, W. Holtzmann, Y. Zhang, F. Fan, T. Taniguchi, K. Watanabe, Y. Ran, T. Cao, L. Fu, D. Xiao, W. Yao, and X. Xu, Signatures of fractional quantum anomalous hall states in twisted mote2, *Nature* **622**, 63 (2023).
- [20] Y. Zeng, Z. Xia, K. Kang, J. Zhu, P. Knüppel, C. Vaswani, K. Watanabe, T. Taniguchi, K. F. Mak, and J. Shan, Thermodynamic evidence of fractional chern insulator in moiré mote2, *Nature* **622**, 69 (2023).
- [21] H. Park, J. Cai, E. Anderson, Y. Zhang, J. Zhu, X. Liu, C. Wang, W. Holtzmann, C. Hu, Z. Liu, T. Taniguchi, K. Watanabe, J.-H. Chu, T. Cao, L. Fu, W. Yao, C.-Z. Chang, D. Cobden, D. Xiao, and X. Xu, Observation of fractionally quantized anomalous hall effect, *Nature* **622**, 74 (2023).
- [22] F. Xu, Z. Sun, T. Jia, C. Liu, C. Xu, C. Li, Y. Gu,

- K. Watanabe, T. Taniguchi, B. Tong, J. Jia, Z. Shi, S. Jiang, Y. Zhang, X. Liu, and T. Li, Observation of integer and fractional quantum anomalous hall effects in twisted bilayer  $\text{mote}_2$ , *Phys. Rev. X* **13**, 031037 (2023).
- [23] Z. Lu, T. Han, Y. Yao, A. P. Reddy, J. Yang, J. Seo, K. Watanabe, T. Taniguchi, L. Fu, and L. Ju, Fractional quantum anomalous hall effect in multilayer graphene, *Nature* **626**, 759 (2024).
- [24] L. Chen, T. Mazaheri, A. Seidel, and X. Tang, The impossibility of exactly flat non-trivial chern bands in strictly local periodic tight binding models, *J. Phys. A: Math. Theor.* **47**, 152001 (2014).
- [25] D. L. Bergman, C. Wu, and L. Balents, Band touching from real-space topology in frustrated hopping models, *Phys. Rev. B* **78**, 125104 (2008).
- [26] J.-W. Rhim and B.-J. Yang, Classification of flat bands according to the band-crossing singularity of bloch wave functions, *Phys. Rev. B* **99**, 045107 (2019).
- [27] J.-W. Rhim and B.-J. Yang, Singular flat bands, *Adv. Phys.: X* **6**, 1901606 (2021).
- [28] J.-W. Rhim, K. Kim, and B.-J. Yang, Quantum distance and anomalous landau levels of flat bands, *Nature* **584**, 59 (2020).
- [29] H. Yu, M. Chen, and W. Yao, Giant magnetic field from moiré induced Berry phase in homobilayer semiconductors, *Natl. Sci. Rev.* **7**, 12 (2020).
- [30] The Supplemental Materials contain systematic analysis of SFB, calculation methods, extra results of entanglement spectrum, evolution of charge gap, charge pumping simulation at  $\nu_{\text{sfb}} = 1/3$ , Hartree-Fock calculations of quasiparticle bands, and two-band exact diagonalization calculation results.
- [31] J. Vidal, R. Mosseri, and B. Douçot, Aharonov-bohm cages in two-dimensional structures, *Phys. Rev. Lett.* **81**, 5888 (1998).
- [32] B. Sutherland, Localization of electronic wave functions due to local topology, *Phys. Rev. B* **34**, 5208 (1986).
- [33] C. Xu, J. Li, Y. Xu, Z. Bi, and Y. Zhang, Maximally localized wannier functions, interaction models, and fractional quantum anomalous hall effect in twisted bilayer  $\text{MoTe}_2$ , *Proc. Natl. Acad. Sci. U.S.A.* **121**, e2316749121 (2024).
- [34] Q. Niu, D. J. Thouless, and Y.-S. Wu, Quantized hall conductance as a topological invariant, *Phys. Rev. B* **31**, 3372 (1985).
- [35] H. Li and F. D. M. Haldane, Entanglement spectrum as a generalization of entanglement entropy: Identification of topological order in non-abelian fractional quantum hall effect states, *Phys. Rev. Lett.* **101**, 010504 (2008).
- [36] M. P. Zaletel, R. S. K. Mong, and F. Pollmann, Topological characterization of fractional quantum hall ground states from microscopic hamiltonians, *Phys. Rev. Lett.* **110**, 236801 (2013).
- [37] S. Kourtis, T. Neupert, C. Chamon, and C. Mudry, Fractional chern insulators with strong interactions that far exceed band gaps, *Phys. Rev. Lett.* **112**, 126806 (2014).
- [38] A. G. Grushin, J. Motruk, M. P. Zaletel, and F. Pollmann, Characterization and stability of a fermionic  $\nu = 1/3$  fractional chern insulator, *Phys. Rev. B* **91**, 035136 (2015).
- [39] N. Morales-Durán, J. Wang, G. R. Schleder, M. Angeli, Z. Zhu, E. Kaxiras, C. Repellin, and J. Cano, Pressure-enhanced fractional chern insulators along a magic line in moiré transition metal dichalcogenides, *Phys. Rev. Res.* **5**, L032022 (2023).
- [40] R. Roy, Band geometry of fractional topological insulators, *Phys. Rev. B* **90**, 165139 (2014).
- [41] Z. Guo, X. Lu, B. Xie, and J. Liu, Fractional chern insulator states in multilayer graphene moiré superlattices, *Phys. Rev. B* **110**, 075109 (2024).
- [42] J. Herzog-Arbeitman, Y. Wang, J. Liu, P. M. Tam, Z. Qi, Y. Jia, D. K. Efetov, O. Vafek, N. Regnault, H. Weng, Q. Wu, B. A. Bernevig, and J. Yu, Moiré fractional chern insulators. ii. first-principles calculations and continuum models of rhombohedral graphene superlattices, *Phys. Rev. B* **109**, 205122 (2024).
- [43] J. Dong, T. Wang, T. Wang, T. Soejima, M. P. Zaletel, A. Vishwanath, and D. E. Parker, Anomalous hall crystals in rhombohedral multilayer graphene i: Interaction-driven chern bands and fractional quantum hall states at zero magnetic field, *arXiv:2311.05568* (2023).
- [44] Z. Dong, A. S. Patri, and T. Senthil, Theory of fractional quantum anomalous hall phases in pentalayer rhombohedral graphene moiré structures, *arXiv:2311.03445* (2023).
- [45] S. Okamoto, N. Mohanta, E. Dagotto, and D. Sheng, Topological flat bands in a kagome lattice multiorbital system, *Commun. phys.* **5**, 198 (2022).
- [46] N. R. Cooper, Optical flux lattices for ultracold atomic gases, *Phys. Rev. Lett.* **106**, 175301 (2011).
- [47] Y. Aharonov and A. Stern, Origin of the geometric forces accompanying berry's geometric potentials, *Phys. Rev. Lett.* **69**, 3593 (1992).